materials

MDPI

Article

Effects of Adhesive Bond-Slip Behavior on the Capacity of Innovative FRP Retrofits for Fatigue and Fracture Repair of Hydraulic Steel Structures

Christine M. Lozano * and Guillermo A. Riveros *

United States Army Corps of Engineers Engineer Research and Development Center, Vicksburg, MS 39180-6199, USA

* Correspondence: Christine.M.Lozano@usace.army.mil (C.M.L.); Guillermo.A.Riveros@usace.army.mil (G.A.R.)

Received: 20 April 2019; Accepted: 4 May 2019; Published: 8 May 2019

Abstract: Over eighty percent of the navigation steel structures (NSS) in the United States have highly deteriorated design boundary conditions, resulting in overloads that cause fatigue cracking. The NSSs' highly corrosive environment and deterioration of the protective system accelerate the fatigue cracking and cause standard crack repair methods to become ineffective. Numerous studies have assessed and demonstrated the use of carbon fiber reinforced polymers (CFRP) to rehabilitate aging and deteriorated reinforced concrete infrastructure in the aerospace industry. Due to the increase of fatigue and fracture failures of NSS and the shortage of research on CFRP retrofits for submerged steel structures, it is imperative to conduct research on the effects of CFRP repairs on NSS, specifically on the adhesive's chemical bonding to the steel substrate. This was accomplished by developing a new analytical algorithm for CFRP bond-slip behavior, which is based on Volkersen's contact shear single lap joint (SLJ) connection. The algorithm was validated by experimental results of fatigue center-cracked large steel plates repaired with CFRP patches. The state of stresses at the crack tip are largely influenced by a combination of the crack tip plasticity radius and overall bond surface area.

Keywords: carbon fibers; fatigue and fracture repairs; hydraulic steel structures; extended finite element; bond-slip; traction-separation; cohesive damage

1. Introduction

Over eighty percent of the navigation steel structures (NSS) within the United States are near to or exceeding their design life [1–3]. Due to deterioration over time and cyclic operation in submerged, highly corrosive environments, NSSs are experiencing fatigue and cracking. For the majority of their life, NSSs are mostly submerged in murky water, therefore the fatigue and fractures, most occurring in the lower/submerged portion of the NSS, go unobserved until they lead to a failure or a scheduled inspection or maintenance. For example, in 2014, Pickwick Lock and Dam operation's staff began to observe longer pool rise times and noise, prompting an inspection. The inspection required a full dewater of the valve. During the inspection, a full fracture of the welded connection of the strut arm's wide flange was discovered and repaired. The implemented repair was a worse fatigue life category detail that required replacement only two years later. An unscheduled operation stoppage costs the U.S. Army Corps of Engineers 1–3 million dollars per day [4–6]. As time passes with gates kept in operation, and no yearly maintenance, the probability of a fatigue and fracture failure and unscheduled stoppage increases linearly [4,7].

The majority of fatigue and fracture repair methods were developed for Mode I cracking in the bridge industry [8–11]. Due to the mixed mode stress states and submerged environment, NSSs

require a different repair method. NSSs require a repair or retrofit that can operate in a submerged environment, will not require further welding or holes (potentials for new crack growth), and is flexible enough to be applied to the lock gate's many different geometrical sections.

Over the past five years, several NSSs' have had fatigue and fractures repaired with a new repair method, carbon fiber reinforced polymer (CFRP) patches [8,9]. This research is part of a five-year project to extend the useful fatigue life of NSS. The conclusion of this research is to develop guidelines to enhance the fatigue life of NSS, which will be incorporated in USACE design memorandums. CFRP has a high strength capacity, low density, and is versatile, making it ideal for fatigue and fracture repairs [10]. To implement the repairs, a lock chamber must be dewatered and the metal section grinded to the base metal, ending with the application of the CFRP composite. The patches are applied to the cracked section using a high-strength adhesive. The adhesive itself is weaker than the steel or CFRP. Therefore, the adhesive's bond strength and behavior are foundational to the overall performance of the CFRP retrofit. This article will describe the bond behavior between steel and adhesive.

This article develops an analytical equation, utilizing Volkersen's contact shear single lap joint (SLJ) connection [12], to determine the fatigue life increase due to the strength contribution of CFRP in the x and y directions. During crack growth, contact shear stresses are developed in the x and y directions, due to the x and y stresses generated by the crack.

1.1. Fatigue and Fracture

Fractures are a separation of a material due to the applied stresses; fatigue and fractures are developed by cyclic stresses over time. These cyclic stresses can be below the yielding point of the material, but as the energy accumulates, it can overcome the capacity of the cohesion energy of the material. The cohesion energy of a material is experimentally determined and commonly expressed as Griffith's energy release rate threshold (Gth). Manufactured materials are a combination of atoms that have an overall capacity known as the critical energy release rate (Gc). The Gth governs the initial fracture of atomic bonds, while the Gc governs the ultimate exponential crack propagation. In linear elastic fracture mechanics (LEFM), there are three stages of fatigue crack propagation: Stage I, Stage II, and Stage III (Figure 1). Stage I marks the portion before the crack initiates and Stage III is when the crack has reached the Gc of the material and propagates exponentially (Figure 1). In between these two capacities is the section known as Stage II (Figure 1); this is where the crack propagates in a predictable and linear fashion [11,13]. It should also be noted that environmental factors, such as corrosion, play an important role in crack propagation by weakening the material causing faster crack growth [11,13].

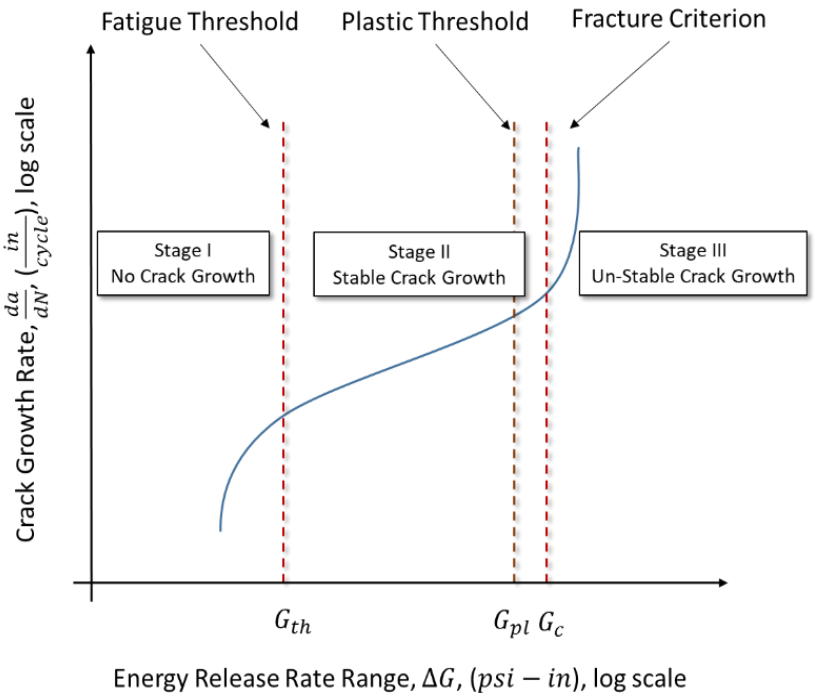

Figure 1. Energy release rate crack growth stages.

Over the past several decades, numerous studies have derived numerous methods to describe fatigue and fracture stress and propagation [11,13]. For this article, Griffith's energy release rate [11], Equation (1), determines the LEFM near-field stresses, Equations (2)–(4), [11], while Paris Law crack propagation [11], Equation (5), calculates the number of cycles, dN, required to propagate a crack over a given distance, da, depending on the material constants C and m.

$$G = \frac{\sigma^2{}_a \pi a}{E} \tag{1}$$

$$\sigma_x = \frac{EG}{\sqrt{2\pi r}} \cos\left(\frac{1}{2}\theta\right)\left(1 - \sin\left(\frac{1}{2}\theta\right)\sin\left(\frac{3}{2}\theta\right)\right) \tag{2}$$

$$\sigma_y = \frac{EG}{\sqrt{2\pi r}} \cos\left(\frac{1}{2}\theta\right)\left(1 + \sin\left(\frac{1}{2}\theta\right)\sin\left(\frac{3}{2}\theta\right)\right) \tag{3}$$

$$\tau_{xy} = \frac{EG}{\sqrt{2\pi r}} \sin\left(\frac{1}{2}\theta\right)\left(\cos\left(\frac{1}{2}\theta\right)\cos\left(\frac{3}{2}\theta\right)\right) \tag{4}$$

$$\frac{da}{dN} = C\Delta G^m \tag{5}$$

In Equations (1)–(5), G is the strain energy release rate, σ_a is the applied far-field stress, a is the crack length (for a center crack, it is equal to the half-crack length), E is the Young's modulus of the material; σ_x, σ_y, and τ_{xy} are the near-field stresses at the crack tip; r is the crack tip plasticity radius; and θ is the angle at which σ_a is applied.

1.2. CFRP Fatigue and Fracture Repairs

Due to their low density and high strength capacity, CFRP have become a popular method of strengthening and repairing existing structures [9,14]. In recent years, the United States Army Corps of Engineers (USACE) has developed a method to repair NSS with CFRP patches (Figure 2) [8,9]. However, there is still a need to fully understand the chemical bond between steel and CFRP in large steel structures, as most analytical work has been implemented on above ground structures, such as

bridges, buildings, and aircrafts [15]. The majority of analytical studies investigate the crack growth behavior of a beam in bending [16–18]. Few analytical studies combine the crack growth behavior with the bond-slip behavior of the CFRP patch repairs [19–23].

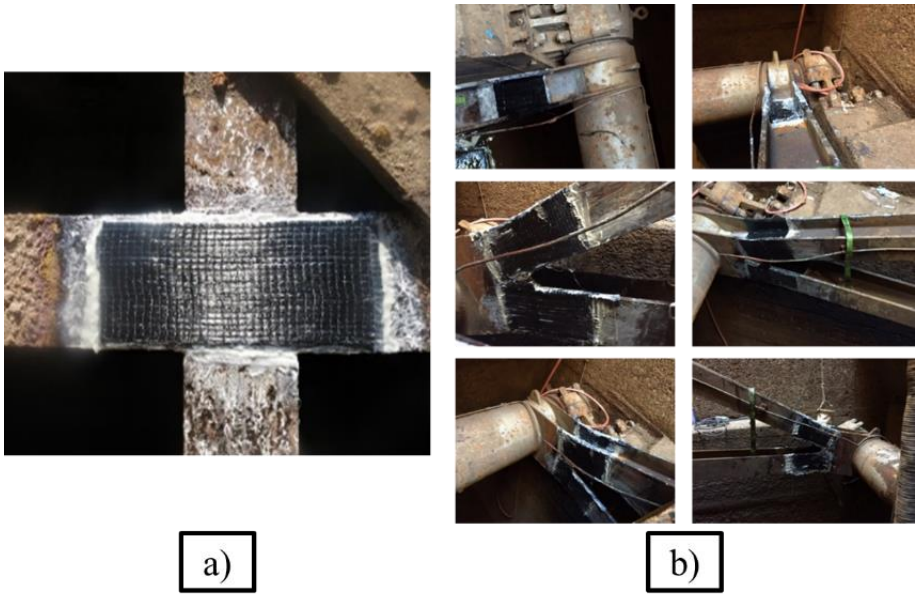

Figure 2. Implemented carbon fiber reinforced polymer (CFRP) repairs. (**a**) Miter gate flange. (**b**) Tainter valve strut arm.

This paper utilizes the experimental results reported in [8] to validate the analytical model. The analytical model is based on the bond contact shear stresses of a single lap joint [12].

1.3. Bond

The bonding of two objects allows the transfer of forces through either objects' surface interface and creates a composite section [24] Adhesives are a common method of joining two surfaces. As long as the applied stresses are below the adhesive's capacity, the bonded section behaves as a composite. This behavior is beneficial for fatigue crack repair with CFRP patches, over the cracked area, as the overall stress capacity of the system is raised by the addition of the CFRP's high tensile capacity [25]. This repair methodology introduces an additional strength capacity, reducing the mean stress range at the crack tip [26–28].

The majority of studies of the bond behavior of CFRP for crack repair or strengthening a section have been developed for concrete [10,18,23,25]. Some new research has been conducted to describe the behavior of steel and CFRP [19,27,29–34]. The majority of the research focuses on only one-directional shear behavior on small scale specimens.

Several analytical models have been developed to describe the contact shear forces developed between two surfaces (adherends) bonded together by an adhesive as a single lap joint (SLJ). Each analytical model makes certain assumptions that govern the resulting equation. Table 1 gives an overview of the previously mentioned analytical models and their assumptions. In 1938, Volkersen derived a contact shear equation that accounted for the tensile elastic deformation of the adherends and shear-only deformation of the adhesive [12,20]. Volkersen's model results in a non-uniform shear stress distribution that is greatest at the ends of the bond and lowest in the middle. Most SLJ bonds develop an eccentricity, due to the adhesive's thickness, developing a bending moment. Several linear elastic extensions to Volkersen's initial bond behavior analytical model were developed by Goland and Reissner, Frostig et al., Hart-Smith, and Bigwood and Crocombe to model the bending moment and subsequent peeling [20,21].

Table 1. Summary of common bond shear analytical models and their common assumptions [21].

Analytical Model	Assumptions				
	Linear Elastic	Deformation	Bending	Transverse Stress	Type of Joint [1]
Volkersen	x	Shear only		Equal	SLJ & DLJ
Goland and Reissner	x	Shear & Normal	x	Equal	SLJ & DLJ
Frostig et al.	x	Shear & Normal	x	Equal	SLJ & DLJ
Hart-Smith	x	Shear & Normal	x	Equal	SLJ & DLJ
Bigwood and Crocombe	x	Shear & Normal	x	Equal	Multiple Configuration

[1] Types of joints: Single Lap Joint (SLJ) and Double Lap Joint (DLJ).

2. Methods

This paper's investigation of bond-slip is based on the observations made during testing of a large-scale plate with and without CFRP patch repairs (Figure 3 and Table 2). The article "Underwater Large-Scale Experimental Fatigue Assessment of CFRP-Retrofitted Steel Panels" by Mahmoud et al. gives a full description of the experimental setup and results [8]. During experimentation, Hudco Formula 3200 and Tyfo S epoxy were tested. Hudco Formula 3200 has the ability to cure underwater, while Tyfo S requires dry conditions for curing. The authors in [8] describe how this adhesive is not ideal to increase fatigue life, due to Hudco Formula 3200's lower strength capacity and faster debonding compared to Tyfo S. The experimental setup was conducted under a Mode I loading of 55 MPa, as reported in [8]. NSSs, such as tainter valves and tainter gates, are subjected to pure Mode I loading.

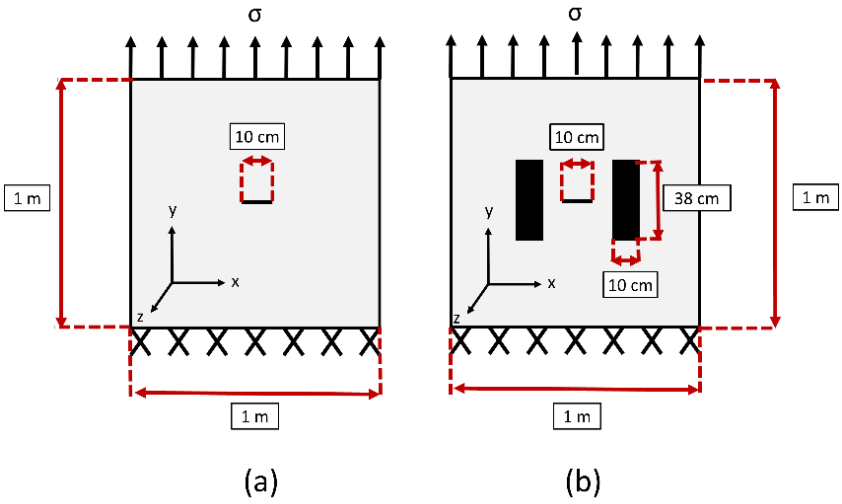

Figure 3. Large-scale steel plate specimen configuration (**a**) with CFRP Repairs; (**b**) without CFRP Repairs.

Table 2. Material properties.

Mechanical Property	Steel	Tyfo SCH-41 (Carbon Fiber) [35]	Tyfo S (Adhesive) [36]
Ex [1] (Gpa)	-	5.93	-
Ey [1] (Gpa)	206	82.7	2.9
Gxy (Gpa)	-	29.5	1.03
ε	-	0.0085	-
σy (Gpa)	344.7	82	-
τu (Gpa)	-	-	1.69×10^{-2}
Gc (Gpa) (Fracture Energy)	-	-	2.10×10^{-7}

[1] The x and y denote the latitudinal and longitudinal directions, respectively.

The CFRP repair method reported in [8] ensured a seamless/no-cold-joint composite of adhesive and CFRP. Therefore, the only bond interface is between the made-up composite and the steel, since the adhesive fully integrates with the CFRP and has a negligible thickness [8].

Analytical

The CFRP was fully saturated when it was adhered to the steel's surface. This condition eliminated any joints between the CFRP and the adhesive and created a very thin interface between the steel and the CFRP of even stress distribution and no bending moment. The adhesive is also a very brittle adhesive, allowing hardly any deformation. Based on the installation and experimental observations, Volkersen's shear interface equation was deemed satisfactory. Volkersen's bond shear derivation is given by Equations (6)–(10).

$$\tau = \frac{P}{bl}\left(\frac{w}{2}\right)\left(\frac{\cosh(wX)}{\sinh\left(\frac{w}{2}\right)}\right) + \frac{\varphi - 1}{\varphi + 1}\left(\frac{w}{2}\right)\left(\frac{\sinh(wX)}{\cosh\left(\frac{w}{2}\right)}\right) \tag{6}$$

$$w = \sqrt{(1+\varphi)\vartheta} \tag{7}$$

$$\varphi = \frac{t_t}{t_b} \tag{8}$$

$$\vartheta = \frac{G_a l^2}{E_t t_t t_a} \tag{9}$$

$$X = \frac{x}{l}, \quad -\frac{1}{2} \le X \le \frac{1}{2} \tag{10}$$

where τ is the interface shear; P is the applied load; b is the width of the bond; l is the full overlap; w, φ, and ϑ are defined in Equations (7)–(9), respectively; t_t, t_b, and t_a are the thicknesses of the top adherend, bottom adherend, and adhesive respectively; G_a is the shear modulus of the adhesive, E_t is the Young's modulus of the CFRP adherend; and X is the distance where the shear is being calculated from the center. Figure 4 shows the different dimensions and layers considered for the analytical model.

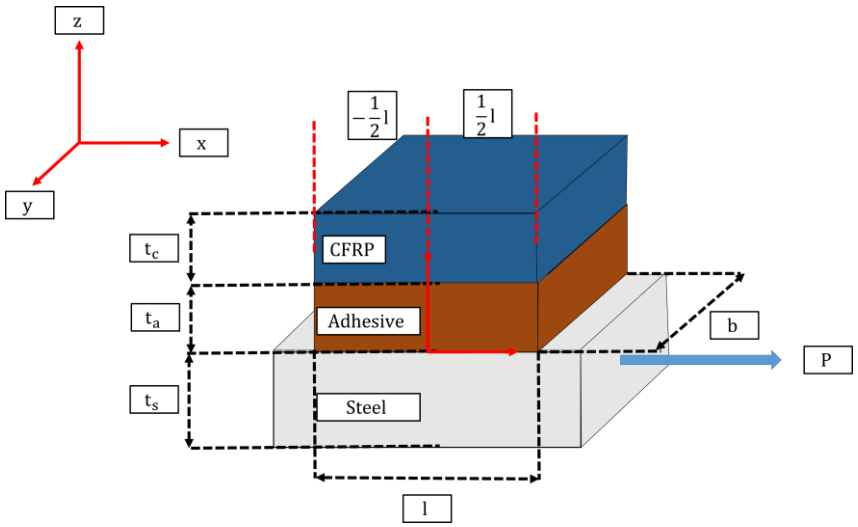

Figure 4. Diagram of single lap joint.

This investigation utilized Volkersen's equation for the contact shear stress, based on the following assumptions. First, the two adherends are highly rigid and experience linear elastic behavior. Second, there is no eccentricity of the adherends. Third, shear and normal stresses of the adhesive are constant through the thickness of the adhesive. Fourth, linear elastic Mode I crack propagation is utilized. Fifth,

there is localized debonding of the adhesive at the crack tip as the crack propagates under the CFRP patch. Finally, the fatigue and fracture is described only for linear crack growth.

The steps taken to determine the contact shear stresses as the crack propagated are shown in Figure 5. First, the current strain energy release rate, G, was calculated from the externally applied load as the crack grew, using Griffith's energy theorem (Equation (1)). As a Mode I crack propagates, it develops near-field stresses that can be split into the x and y directions, using Equations (2) and (3) (Figure 5). Then, these x and y stresses, minus the stiffness contribution of the CFRP patch, respectively, result in an x- and y-applied force, used in the Volkersen's equation (Equation (6)) (Figure 5).

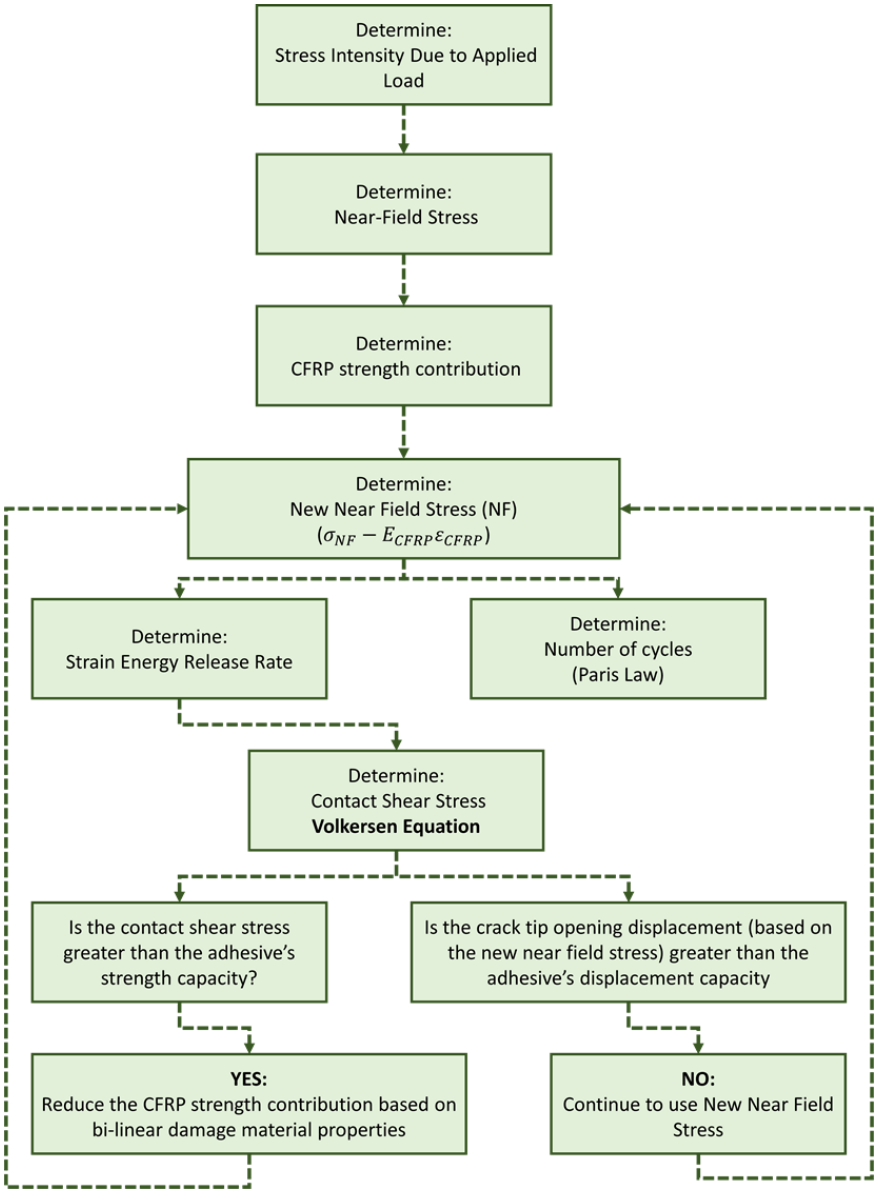

Figure 5. Algorithm of analytical model.

To determine the contact shear stress, Volkersen's equation (Equation (6)) utilizes the total surface area of the bond in an SLJ. However, the localized bond stresses of the CFRP/steel interface require a surface area of 0.5% of the total surface area. This reduction in area was applied to Volkersen's (Equation (6)) in both the x and y directions. If the shear stress in the x and y, respectively, was less than the adhesive's capacity, then there was no debonding and no bi-linear reduction in the CFRP's stiffness contribution. However, if the shear stress was greater than the adhesive's capacity, then the

CFRP's stiffness contribution was reduced. Finally, a new strain energy release rate, G, was calculated with the resultant of the x and y stress to determine the change in cycles as the crack grew, using Paris Law (Equation (5)).

3. Results and Discussion

Figure 6 shows the cycles versus crack length comparison of the experimental and analytical results for a center through crack large plate with and without CFRP patches. For the unrepaired specimen, the analytical and experimental results match up perfectly, until 350,000 cycles. Then the curves diverge as they approach the unstable crack growth region (Region III of Paris Law) [11]. For the repaired specimen, the results begin to diverge at 375,000 cycles, indicating that during the stable crack growth, the analytical model behaves according to the experimental results. The fatigue life improvement at the beginning of the unstable crack growth rate was 30% and 25% for the experimental and analytical, respectively. Figure 6 also shows a 38% and 30% fatigue life improvement from the experiments and analytical model at fracture, respectively (Figure 6).

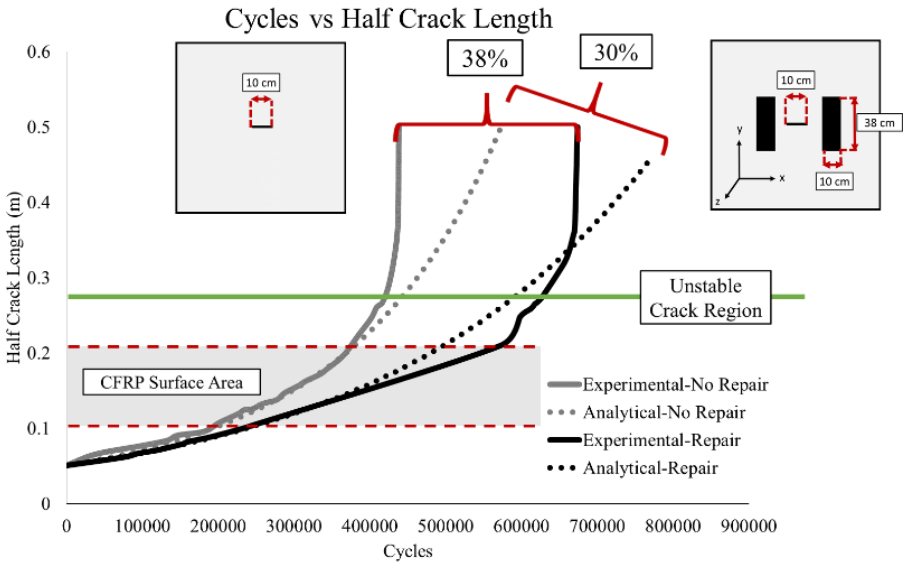

Figure 6. Cycles vs. half crack length results.

To verify the performance of the analytical model, an additional validation comparing the crack length vs. far-field stresses was performed (Figure 7). For the unrepaired specimen, there is a divergence between the experimental and analytical results as the gauge location is reached. The divergence can be attributed to the sensitivity of the r parameter in the near-field stress equation. However, the stresses converged as the crack approached the strain gauge. The stresses, for the repaired specimen, calculated by the analytical bond model, show a good correlation with the experimental results until the crack growth approaches the strain gauge. The divergence between the repaired experimental and analytical stresses is due to non-linear crack tip plasticity.

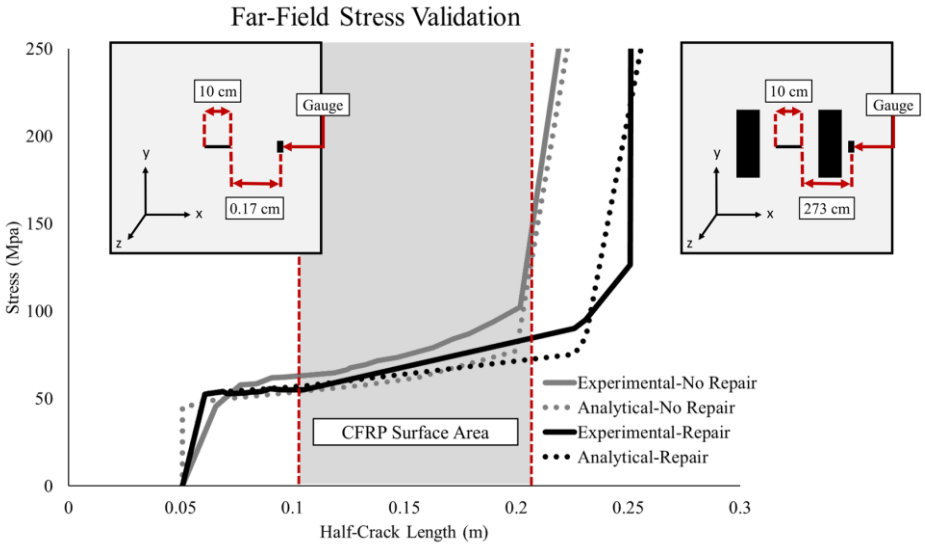

Figure 7. Far-field stress result.

4. Conclusions

This paper develops an analytical expansion of Volkersen's SLJ model [12] to describe the fatigue life improvement of CFRP repairs on cracked steel sections, based on bond-slip behavior. The algorithm required the following assumptions:

- The two adherends are highly rigid and experience linear elastic behavior;
- There is no eccentricity of the adherends;
- Shear and normal stresses of the adhesive are constant through the thickness of the adhesive;
- Linear elastic Mode I crack propagation is utilized;
- The occurrence of the adhesive's localized debonding at the crack tip as the crack propagates under the CFRP patch;
- Fatigue and fracture linear crack growth.

The assumptions allowed the determination of localized debonding, based on the applied far-field stresses.

The analytical model was validated against the experimental number of cycles vs. crack length and far-field stresses vs. crack length data. The cycles vs. crack length results demonstrated a fatigue life improvement of 25% at the start of the unstable region and 30% at fracture. Experimental far-field stresses supplied further validation. It was noted that the unrepaired analytical results diverged from the experimental results due to the sensitivity in the r variable of the near-field stresses at the crack tip. The repaired analytical model's stress results demonstrated a good correlation with the experimental results until the crack began to approach the strain gauge location. The divergence between the repaired experimental and analytical stresses is due to non-linear crack tip plasticity. The analytical model was determined to capture the extended fatigue life behavior of CFRP repairs of steel cracking, which have been proven to improve the fatigue life in NSS by [8,9].

Author Contributions: The work for this article was completed by C.M.L. and G.A.R.; Conceptualization, C.M.L. and G.A.R.; methodology, C.M.L.; validation, C.M.L. and G.A.R.; formal analysis, C.M.L.; investigation, C.M.L. and G.A.R.; resources, G.A.R.; data curation, C.M.L.; writing—original draft preparation, C.M.L.; writing—review and editing, G.A.R.; visualization, C.M.L. and G.A.R.; supervision, G.A.R.; project administration, G.A.R.; funding acquisition, G.A.R.

Funding: The authors gratefully acknowledge the funding from the Engineer Research and Development Center, Navigations System Research Program. The authors thank the Information Technology Laboratory Director, Dr. David Horner and the Chief of Engineers of the US Army Corps of Engineers for permission to publish this paper.

Conflicts of Interest: The authors declare no conflict of interest. The funders had no role in the design of the study; in the collection, analyses, or interpretation of data; in the writing of the manuscript, or in the decision to publish the results.

References

1. Riveros, G.A.; Arredondo, E. Predicting Future Deterioration of Hydraulic Steel Structures with Markov Chain and Multivariate Samples of Statistical Distributions. *J. Appl. Math.* **2014**, *2014*, 360532. [CrossRef]
2. Mahmoud, H.; Chulahwat, A.; Riveros, G. Fatigue and Fracture Life-Cycle Cost Assessment of a Miter Gate with Multiple Cracks. *Eng. Fail. Anal.* **2018**, *83*, 57–74. [CrossRef]
3. Riveros, G.A.; Rosario-Pérez, M.E. Deriving the Transition Probability Matrix Using Computational mechanics. *Eng. Comput.* **2018**, *35*, 692–709. [CrossRef]
4. Grier, D. *The Declining Reliability of the U.S. Inland Waterway System*; U.S. Army Corps of Engineers Institute for Water Resources: Alexandria, VA, USA, 2005.
5. Grossardt, T.; Bray, L.; Burton, M. *Inland Navigation in the United States an Evaluation of Economic Impacts and the Potential Effects of Infrastructure Investment*; National Waterways Foundation: Washington, DC, USA, 2014.
6. Litz, J.; Frank, J. *Retaining the Value of the U.S. Inland Waterways System*; U.S. Army War College: Carlisle, PA, USA, 2017.
7. Kruse, C.J.; Ellis, D.; Protopapas, A.; Norboge, N. *New Approaches for U.S. Lock and Dam Maintenance and Funding*; Texas Transportation Institute: College Station, TX, USA, 2012; pp. 1–127.
8. Mahmoud, H.N.; Riveros, G.A.; Memari, M.; Valsangkar, A.; Ahmadi, B. Underwater Large-Scale Experimental Fatigue Assessment of CFRP-Retrofitted Steel Panels. *J. Struct. Eng.* **2018**, *144*, 04018183. [CrossRef]
9. Riveros, G.A.; Mahmoud, H.; Lozano, C.M. Fatigue repair of underwater navigation steel structures using Carbon Fiber Reinforced Polymer (CFRP). *Eng. Struct.* **2018**, *173*, 718–728. [CrossRef]
10. Nor, N.M.; Boestamam, M.H.A.; Yusof, M.A. Carbon Fiber Reinforced Polymer (CFRP) as Reinforcement for Concrete Beam. *Int. J. Emerg. Technol. Adv. Eng.* **2013**, *3*, 6–10.
11. Barsom, J.; Rolfe, S. *Fracture and Fatigue Control in Structures*, 3rd ed.; ASTM International: West Conshohocken, PA, USA, 1999; ISBN 78-0750673150.
12. Volkersen, O. Die Niektraftverteilung in Zugbeanspruchten mit Konstanten Laschenquerschritten. *Luftfahrtforschung* **1938**, *15*, 41–47.
13. Freudenthal, A.M. Fatigue and fracture mechanics. *Eng. Fract. Mech.* **1973**, *5*, 403–414. [CrossRef]
14. Lozano, C. Development of Pre-Stressed Retrofit Strategies for Mitigating Fatigue Cracking in Steel Waterway Lock Gate Components. Master's Thesis, University of Arkansas, Fayetteville, Arkansas, 2017.
15. Wang, H.-T.; Wu, G.; Jiang, J.-B. Fatigue Behavior of Cracked Steel Plates Strengthened with Different CFRP Systems and Configurations. *J. Compos. Constr.* **2016**, *20*, 04015078. [CrossRef]
16. ElSafty, A.; Graeff, M. *The Repair of Damaged Bridge Girders with Carbon-Fiber-Reinforced Polymer "CFRP" Laminates*; University of North Florida: Jacksonville, FL, USA, 2012.
17. Dawood, M.; Rizkalla, S. Development of a Carbon Fiber Reinforced Polymer System for Strengthening and Repair of Steel Bridges and Structures; Culture for Effective Design of Structures. In Proceedings of the 2nd Canadian Conference on Effective Design of Structures, Hamilton, ON, Canada, 20–23 May 2003.
18. Klaiber, F.W.; Wipf, T.J.; Kempers, B.J. Repair of Damaged Prestressed Concrete Bridges Using CFRP. In Proceedings of the 2003 Mid-Continental Transportation Research Symposium, Ames, IA, USA, 21–22 August 2003.
19. Chandrathilaka, E.R.K.; Gamage, J.C.P.H.; Fawzia, S. Numerical Modelling of Bond Shear Stress Slip Behavior of CFRP/Steel Composites Cured and Tested at Elevated Temperature. *Compos. Struct.* **2019**, *212*, 1–10. [CrossRef]
20. Da Silva, L.F.; das Neves, P.J.; Adams, R.D.; Spelt, J.K. Analytical Models of Adhesively Bonded Joints-Part I: Literature Survey. *Int. J. Adhes. Adhes.* **2009**, *29*, 319–330. [CrossRef]
21. Da Silva, L.F.; das Neves, P.J.; Adams, R.D.; Wang, A.; Spelt, J.K. Analytical Models of Adhesively Bonded Joints-Part II: Comparative Study. *Int. J. Adhes. Adhes.* **2009**, 331–341. [CrossRef]
22. Fayyadh, M.M.; Razak, H.A. Analytical and Experimental Study on Repair Effectiveness of CFRP Sheets for RC Beams. *J. Civ. Eng. Manag.* **2014**, *20*, 21–31. [CrossRef]

23. Rosenboom, O.; Rizkalla, S. Analytical Modeling of Flexural Debonding in CFRP Strengthened Reinforced or Prestressed Concrete. In Proceedings of the 8th International Symposium on Fiber Reinforced Polymer Reinforcement for Concrete Structures (FRPRCS-8), Patras, Greece, 16–18 July 2007.
24. Adderley, C.S. Adhesive Bonding. *Mater. Des.* **1988**, *9*, 287–293. [CrossRef]
25. Alkhrdaji, T. Strengthening of Concrete Structures Using FRP Composites. *Struct. Mag.* **2015**, *12*, 18–20.
26. Wang, H.-T.; Wu, G.; Pang, Y.-Y. Theoretical and Numerical Study on Stress Intensity Factors for FRP-Strengthened Steel Plates with Double-Edged Cracks. *Sensors* **2018**, *18*, 2356. [CrossRef]
27. Liu, H.B.; Xiao, Z.G.; Zhao, X.L. Fracture Mechanics Analysis of Cracked Steel Plates Repaired with Composite Sheets. In Proceedings of the Asia-Pacific Conference on FRP in Structures (APFIS 2007), Hong Kong, China, 12–14 December 2007.
28. Ghafoori, E.; Motavalli, M. A Retrofit Theory to Prevent Fatigue Crack Initiation in Aging Riveted Bridges Using Carbon Fiber-Reinforced Polymer Materials. *Polymers* **2016**, *8*, 308. [CrossRef]
29. Yang, Y.; Biscaia, H.; Chastre, C.; Silva, M.A.G. Bond Characteristics of CFRP-to-steel Joints. *J. Constr. Steel Res.* **2017**, *138*, 401–419. [CrossRef]
30. Al-Mosawe, A.; Al-Mahaidi, R. Bond Characteristics between Steel and CFRP Laminate under Impact Loads. In Proceedings of the 23rd Australasian Conference on the Mechanics of Structures and Materials, Byron Bay, Australia, 9–12 December 2014.
31. Schnerch, D.; Dawood, M.; Rizkalla, S.; Sumner, E.; Stanford, K. Bond Behavior of CFRP Strengthened Steel Structures. *Adv. Struct. Eng.* **2006**, *9*, 805–817. [CrossRef]
32. Fawzia, S.; Karim, M.A. Investigation into the Bond between CFRP and Steel Plates. *Int. J. Civ. Environ. Eng.* **2009**, *3*, 5.
33. Wu, C.; Zhao, X.-L.; Al-Mahaidi, R.; Duan, W.H. Experimental Study on Bond Behaviour between UHM CFRP Laminate and Steel. In *Advances in FRP Composites in Civil Engineering*; Ye, L., Feng, P., Yue, Q., Eds.; Springer: Berlin/Heidelberg, Germany, 2011; pp. 890–893.
34. Sahin, M.; Dawood, M. Experimental Investigation of Bond between High-Modulus CFRP and Steel at Moderately Elevated Temperatures. *J. Compos. Constr.* **2016**, *20*, 04016049. [CrossRef]
35. Tyfo® SCH-41 Composite Using Tyfo® S Epoxy 2015. Available online: https://www.aegion.com/-/media/Files/Fyfe/2013-Products/Tyfo%20SCH%2041.ashx (accessed on 11 February 2019).
36. Tyfo® S Saturant Epoxy 2015. Available online: http://fyfeasia.com/-/media/Files/Fyfe/2013-Products/Tyfo%20S%20Epoxy.ashx?la=en (accessed on 11 February 2019).